Journal of Materials Chemistry C

Accepted Manuscript

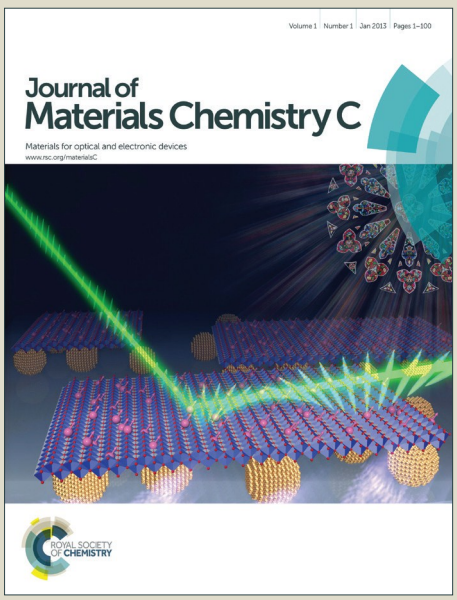

ROYAL SOCIETY OF CHEMISTRY

www.rsc.org/materialsC

Low temperature synthesis of graphite on Ni films using inductively coupled plasma enhanced CVD

Lanxia Cheng [a,*], Kayoung Yun [b], Antonio Lucero [a], Jie Huang [c], Xin Meng [a], Guoda Lian [a], Ho-Seok Nam [b], Robert M. Wallace [a], Moon Kim [a], Archana Venugopal [c], Luigi Colombo [c], Jiyoung Kim [a,*]

[a] Department of Materials Science and Engineering, The University of Texas at Dallas, 800 W. Campbell Road, Richardson, Texas 75080, USA

[b] School of Advanced Materials Engineering, Kookmin University, Seoul, Korea

[c] Texas Instruments, Dallas, Texas 75080, USA

ABSTRACT

Controlled synthesis of graphite at low temperatures is a desirable process for a number of applications. Here, we present a study on the growth of thin graphite films on polycrystalline Ni films at low temperatures, about 380 °C, using inductively coupled plasma enhanced chemical vapor deposition. Raman analysis shows that the grown graphite films are of good quality as determined by a low I_D/I_G ratio, ~0.43, for thicknesses ranging from a few layers of graphene to several nanometers thick graphitic films. The growth of graphite films was also studied as a function of time, precursor gas pressure, hydrogen concentration, substrate temperature and plasma power. We found that graphitic films can be synthesized on polycrystalline thin Ni films on SiO_2/Si substrates after only 10 seconds at a substrate temperature as low as 200 °C. The amount of hydrogen radicals, adjusted by changing the hydrogen to methane gas ratio and pressure, was found to dramatically affect the quality of graphite films due to its dual role of as a catalyst and etchant. We also find that a plasma power of about 50W is preferred in order to minimize plasma induced graphite degradation.

Keywords: PECVD, graphene, graphite, Raman, low temperature synthesis

* Corresponding authors: Tel:+1 972-883-6412,
E-mail: jiyoung.kim@utdallas.edu, lanxia.cheng@utdallas.edu

1. Introduction

Nanostructured carbon materials (carbon nanotubes (CNT) and graphene) are being studied as alternatives for future devices and interconnect applications because of their unique properties.[1-7] Recent studies of interconnects in integrated circuits fabricated using CNTs[8, 9] and graphene [10] have demonstrated high breakdown current density, up to 10^9A/cm^2, which is about three orders of magnitude higher than Cu wire interconnects. This, along with their high resistance to electron-migration makes sp^2 carbons appealing for device applications. In this context, it would be desirable to grow graphene, multilayer graphene and graphite at temperatures compatible with silicon device back-end-of-line (BEOL) thermal budgets.

Commercial graphite is largely produced by thermal annealing of petroleum cokes and coal tar pitches in furnaces at very high temperatures, up to 3000 °C.[11] Over the past 10 years in an effort to grow graphene, graphitic film growth at temperatures as high as 1300 °C has been rediscovered.[12] The process takes place by a thermal dissociation of hydrocarbons on transition metal substrates followed by dissolution of the carbon in the metal at high temperature[13-17] followed by segregation and precipitation of the supersaturated carbon upon cooling to form large area and high quality graphitic films. However, the typical temperature at which graphite is formed is not compatible with silicon BEOL thermal budgets. Recently, there have been many reports on the growth of graphite films at reduced temperature using plasma enhanced chemical vapor deposition (PECVD)[18-22] where plasma, instead of heat, is used to dissociate the hydrocarbon sources. PECVD synthesis of large area high quality graphene and few layer graphene films has been reported at ~700 °C on metal substrates such as Cu,[23, 24] Ni[25-27] and Co.[28] However, for some applications, lower growth temperatures are desired in order to integrate sp^2 carbons directly in device flows rather than transferring the films as is currently done for graphene films.

In this work, we present a detailed study on the growth behavior of graphitic films on polycrystalline Ni substrates using inductively coupled plasma enhanced chemical vapor deposition (IC-PECVD). The growth temperature in our work is lower than 475 °C, a temperature range outside of what is reported to be necessary to promote graphitic film growth on Ni by precipitation.[29] Our results strongly suggest that good quality, thick graphite films of several nanometers can be obtained at temperatures as low as 380 °C and growth of sp^2 carbon as observed at temperatures as low as 200 °C. We also studied the influence of the growth conditions, namely growth time, temperature, plasma power and precursor composition on the

quality of graphite. The as-grown graphitic films were then characterized using Raman spectroscopy, scanning electron microscopy (SEM) and X-ray photoelectron spectroscopy (XPS), and transmission electron microscopy (TEM).

2. Experimental

The graphite films were grown on sputtered Ni polycrystalline films (~500nm) on SiO_2 (200 nm)/Si substrate in a commercial PECVD chamber. As schematically shown in Fig. 1, the plasma setup is an ICP generator operating at 13.56 MHz and is mounted on a high vacuum stainless steel chamber, 16 cm above the sample heater. The growth chamber is evacuated using a turbo pump to maintain high vacuum condition around ~10^{-8} Torr and the substrate is placed directly on the heater. Growth of the graphite films was performed as following: 1) the Ni film was annealed at 380 °C in a hydrogen and argon gas environment with a flow ratio of 40:40 standard cubic centimeters per minute (sccm) for 1 hour to clean the Ni surface and to stabilize the Ni microstructure; 2) the Ni surface was then exposed to a mixture of H_2 and Ar plasma for 2 minutes with a plasma power of 50 W and Ar/H_2 flow rate ratio of 40:40 sccm at a total pressure of 20 mTorr; 3) graphite was then grown according the prescribed recipes. The graphite growth conditions such as sample temperature is varied from 200-800 °C; the gas mixture ratio and flow of argon (Ar), hydrogen (H_2) and methane (CH_4) were 40:30:10 or 70:0:10 sccm (the Ar carrier gas is used to dilute the hydrocarbon gas source and stabilize the plasma); and the growth time was varied from 10 s to 2 hrs. Note that all temperatures mentioned in this work are the actual growth temperature calibrated using the thermocouple to ensure the accuracy of the growth temperature for every growth run. After deposition, the samples were cooled down to room temperature over a period of 30 minutes under a 100 sccm continuous flow of Ar. The structure of the graphite films was then analyzed using a Renishaw confocal Raman spectroscopic system with a laser excitation energy of 532 nm in an inVia Reflex spectrometer. The laser power was maintained at ~1.5 mW to avoid local laser overheating.[30] For each sample, Raman spectra of at least three random points (spot size: ~500 nm) were collected. Raman mapping images were recorded at a spot step size of 100 nm over 10 × 10 μm area with a spatial resolution of 200-300 nm. The film composition was also studied by X-ray photoelectron spectroscopy (XPS) using a monochromatic Al Kα (hν = 1486.7 eV) X-ray source equipped with a 7 channel analyzer using a pass energy of 15.0 eV with all scans taken at 45° and spot size of 100 × 100 μm^2 with respect to the sample.[31] The morphology of

the graphite films was studied using Zeiss supra-40 scanning electron microscope (SEM) operated at electron energy of 5.0 kV. The cross-section image of graphite film is obtained on a JEM-ARM200F Transmission Electron Microscope (TEM) operated at 200 kV.

3. Results and discussions

3.1. Effect of deposition time

Fig. 2a shows the Raman spectra of graphite films on a polycrystalline Ni surface as a function of growth time at a growth temperature of 380 ˚C. The graphite films are deposited using methane diluted in Ar at a flow rate ratio of 70:10 sccm and a plasma power of 50W. After a 10 s deposition time, the deposited films show both D and G Raman peaks at ~1342 cm^{-1} and ~1596 cm^{-1} respectively. The D peak is considered as signature of structural defects present in graphene films while the G peak is associated with the formation of sp^2 hybridized carbon network and originates from the doubly degenerate phonon vibrations at the Brillouin zone center.[32-34] Hence, for a very short deposition time, the Raman results show the formation of defective graphitic carbon on the Ni surface. For longer growth times the 2D peak, observed at ~2705 cm^{-1}, starts to appear and becomes stronger. This 2D peak is generated by second-order zone boundary phonon scattering and is sensitive to the c-axis stacking of graphene layers.[34, 35] The appearance of a 2D Raman peak, accompanied by a red shift of the G peak at ~1582 cm^{-1} after 300 s deposition points towards the formation of Bernal stacked few layer graphene films. Furthermore, the decrease of the D peak and the increase of the G peak intensity suggest that the growing film quality improves with growth time. Increasing the deposition time up to 2 hrs causes no distinctive changes in the relative intensity between D and G bands, but the 2D band broadens and changes its shape from symmetric to asymmetric with the FWHM increasing from ~80 to ~94 cm^{-1}, which implies the formation of multilayer graphene films. A similar transition of the initial highly defective graphitic structure to good quality of graphite films has also been observed by other groups at ~800 °C,[21, 24, 26] in which the continuous adsorption of incoming carbon radicals on highly reactive carbon defects, such as grain boundaries or dangling bonds, and graphite edges contributes to the increase of graphite domain size and film thickness.

Fig. 2 b-c present the change in the relative intensity ratios of the D-, G- and 2D-bands, I_D/I_G and I_{2D}/I_G, and their respective FWHM as a function of deposition time. The I_D/I_G peak ratio continuously decreases from ~1.2 to ~0.42 as the deposition time is increased from 10 s to 300 s; concurrently, the peak linewidths of the D- and G-bands become narrower from ~80 to ~53

cm^{-1} and ~85 to ~46 cm^{-1}, respectively; an indication of larger graphite domain size and better structural quality. However, our observation on the evolution of the I_D/I_G ratio as a function of deposition time is opposite to that claimed by Peng *et. al*[29] where extended plasma exposure was found to degrade the graphite film quality at 475 °C. The principal difference that could explain our results from Peng's[29] is chamber geometry as is related to the plasma source. In our case, the use of the IC plasma setup isolates the substrate from direct plasma contact, thereby reducing damage because of the decrease of Ar ion bombarding energy.[36] To confirm the uniformity of the deposited graphite films on Ni substrate, we performed Raman mapping of the graphite films grown for a period of 300 s at a growth temperature of 380 °C. Fig. 3a shows the G peak intensity map across an area of 10 ×10 µm. Fig. 3b shows a HR-TEM cross-section image of a graphite film having a thickness of several tens of nanometers.

3.2. Effect of gas mixture pressure

Hydrogen has been reported to play a role in thermal CVD synthesis of graphene.[37] We find that the same is true in PECVD; Fig. 4 shows the effect of gas source pressure on graphite quality in a hydrogen-free and -rich environment at 380 °C for the same plasma power of 50W and a growth time of 300 s. The gas pressure is adjusted by using a downstream pressure control under different gas flow rates. Fig. 4a shows the Raman spectra of graphite films deposited using an Ar:CH_4 gas mixture (hydrogen-free) at a flow rate ratio of 70:10 sccm. Three Raman peaks, at ~1346, ~1586 and ~2702 cm^{-1}, are observed after 300 s plasma exposure at 10 mTorr, along with a low intensity peak at ~2940 cm^{-1}, referred to as D+G peak, which is believed to be associated with the presence of defective sp^2 sites.[33] Under this condition, both D and G peaks are broad and exhibit similar intensities indicative of the formation of a defective graphite film. Upon increasing the gas pressure to 20 and 50 mTorr, the D peak intensity is reduced, accompanied by the disappearance of the D+G peak. As indicated by the Raman spectra, the corresponding D and G peak intensity ratio I_D/I_G also shows a significant reduction, from ~1.1 to ~0.33, upon gas pressure increase to 50 mTorr from 20 mTorr, shown in Fig. 4 b-d. The FWHM of G peak also decreases from ~62 cm^{-1} to ~40 cm^{-1}, presumably as a result improved lattice ordering of graphitic film. This suggests that the graphite quality improves in the absence of hydrogen presumably as a result of a decrease in graphite etching by hydrogen ions.

In contrast, when hydrogen is introduced using a gas mixture of Ar-H_2-CH_4 (hydrogen-rich) at a flow rate ratio of 30:40:10 sccm, shown in Fig. 4c, the Raman spectra of the graphite films

display an opposite trend in the corresponding D and G peak intensities in reference to those deposited from a hydrogen-free gas source. The increase of the deposition pressure from 10 to 50 mTorr leads to a higher intensity D peak and lower intensity G peak. Accordingly, in Fig. 4 b - d, the I_D/I_G increases from ~0.45 to ~1.05, accompanied by a broadening of the FWHM of G peak from ~38 cm^{-1} to ~79 cm^{-1}. This opposite trend in the I_D/I_G, as a function of deposition pressures is believed to be caused by the variations in the amount of hydrogen species generated under both hydrogen-free and -rich deposition environments. Previous studies have demonstrated that hydrogen can play several complicated roles in growth of graphene by CVD, such as co-catalyst creating active sites for carbon species, *e.g.* CH_x, surface binding and dehydrogenation, passivation of defects and gain boundaries, C-etching, etc..[37, 38] However, during graphite/graphene growth by PECVD, hydrogen species can be effectively supplied by decomposition of methane molecule using plasma,[29, 39] the amount of these hydrogen species generated for graphite deposition can increase gradually when the gas source pressure increases under hydrogen-free condition, which leads to formation of graphite films with large grain size at higher gas pressure. Nevertheless, by adding hydrogen molecules to the gas source, the relative ratio of carbon and hydrogen species can be dramatically increased which can contribute to the formation of hybridized sp^3 CH_x species and passivation of carbon active site for continuous graphene growth. Our Raman results show that at 10 mTorr, the I_D/I_G of films grown under hydrogen-free gas sources is lower than that from hydrogen-rich condition due to the increase in etching of the graphite because of a higher concentration of hydrogen species. These findings suggest that optimizing the hydrogen species concentration is crucial for synthesis of good quality graphite films.

3.3. Effect of deposition temperature

The effect of temperature on the growth of graphite using Ar-CH_4 and Ar-H_2-CH_4 conditions was also studied as a function of temperature in the range of 200 to 800 °C. A plasma power of 50 W was used to generate the carbon radicals and the deposition time was kept constant at 300 s. Fig. 5a - b show Raman spectra of the deposited graphite films. At low growth temperatures, the Raman spectra of the samples grown at 200, 250 and 300 °C show relatively strong and broad D and G bands at ~1355 cm^{-1} and ~1596 cm^{-1}, respectively, along with a weak 2D band at ~2702 cm^{-1} and the intensity ratios of D to G bands, I_D/I_G, are found to be above ~1.0. The presence of very weak 2D peak and high I_D/I_G values are related to the formation of highly defective and small graphitic nanostructures. At low growth temperatures, the mobility of reactive carbon species is relatively low, which could restrict carbon species from forming

large sp^2 networks. At temperatures above 380 °C, the Raman D-band shifts toward ~1584 cm^{-1}, and the band intensity decreases, causing the corresponding I_D/I_G ratio to gradually decrease from ~0.45 to nearly ~0.002 as the growth temperature is increased to 800 °C. In addition, the FWHM of the G band becomes narrower, from ~64 to ~30 cm^{-1}, close to that of graphite;[40] and evidences that the crystallinity of the growing film improves with increasing growth temperature. The Raman data of the multilayer graphene films grown at ~ 500 °C agrees well with those reported in other studies[41, 42] conducted at similar temperatures. It is worth noting that our demonstration on the successful growth of graphitic films at temperature as low as 200 °C is in contrast to what is reported by Peng's group[29] who claimed that graphene layers fail to deposit on the Ni surface because of the negligible carbon dissolution below 475 °C. Batzill *et al.* also suggest that Ni_2C carbide phase formed favorably at low carbon concentration below 480 °C, which impedes the nucleation and growth of single layer graphene on Ni crystal surface.[43] The results presented in this paper suggest that a different growth mechanism is operative and it is not a dissolution and precipitation mechanisms as is the case in thermal growth of graphene on Ni [14, 37, 44, 45] reported to date, in which the relative high carbon solubility of ~2.7 at% at a temperature of ~1000 °C[46] serves as main driving force for graphene precipitation. At temperatures below 450 °C the carbon solubility drops to 0 at%, close to the value of ~0.001 at% reported for Cu at 1084 °C,[47] and thus the growth mechanism, once a nucleus is formed, is by nucleation and growth of incoming carbon radicals at graphite edges and defects without carbon diffusion from bulk Ni substrate. The quality of the multilayer graphene films grown at a temperature as low as 380 °C is comparable to films deposited at ~500-600 °C by PECVD,[21, 41]Unlike the thermal CVD process on Cu where dehydrogenation of hydrocarbon stops due to the poisoning of the catalyst, a continuous supply of CH_x species is realized by the plasma and these active carbon species can attach to graphene edges (defects) and grain boundaries, leading to the formation of multilayer graphene films.[20, 24, 41, 48] Our results suggest that the deposition of graphitic structure using IC-PECVD methods is not limited to metal surfaces like Ni but perhaps also on other materials, *e.g.* hexagonal 2D materials.

The growth of graphitic films on Ni as a function of temperature was also performed using Ar-H_2-CH_4 gas sources in a hydrogen-rich environment for a plasma excitation power of 50 W and growth time of 300 s. The Raman spectra are shown in supplemental information (SI), Fig. S1. Even though the Raman spectra of these samples demonstrate a similar trend as films grown without hydrogen, the related intensity ratios of D to G bands, I_D/I_G, and the

FWHM of G band are slightly higher. In addition, the etching effect of hydrogen is not obvious at temperatures above 500 °C whereof the graphitic film growth mechanism is dominated by segregation and precipitation mechanism.[14, 44, 45]

To further verify the growth of sp^2 carbon in the temperature range of 200 °C to 800 °C, the composition of these films was characterized using XPS as shown in Fig. 6a. The XPS spectra of the C1s for the films grown at 200, 380 and 800 °C appear to be nearly identical, suggesting the main components of the carbon films are C=C bonded sp^2 structures. However, the Raman spectra, that are more sensitive to structure than XPS, shown in Fig. 6b, indicate that while the films grown at high temperature show a very small D-band and a well-defined 2D band, the films grown at low temperature show a very high D-band and a less developed 2D-band. The microstructure of the Ni, shown in Fig. S2, may not have a large effect on the quality of the growing graphite and the Raman spectra of films grown at different temperatures are shown in the supplemental information (SI) Fig. S1 and Fig. 5.

3.4. Effect of deposition plasma power

Fig. 7 a shows the Raman spectra of graphite films grown for 2 hrs as a function of plasma power at a growth temperature of 380 °C under hydrogen-free conditions. The intensities and FWHMs of the D, G and 2D peaks of graphene films, found at ~1351, ~1581 and ~2703 cm^{-1}, respectively, degraded when the plasma power is increased from 50 to 150W. At low plasma power, below 100W, low defect density graphitic films are observed as evident from the low ratio of D to G peaks, I_D/I_G, of ~0.45, Fig. 7 b. This ratio increases to ~1.0 when the plasma power is increased to 150 W, implying that structural defects are induced by the effects of the plasma, probably hydrogen ion etching, and consequently, the FWHMs of G band broadens from ~37 to ~83 cm^{-1}. The Raman behavior of graphite films grown as a function of plasma power is in agreement with the results reported by Kim *et al*..[39] The plasma power can influence the graphite grain size by controlling the amount of the active species, in particular, the hydrogen ions generated by plasma. Increasing the plasma power can increase the graphene grain size by increasing the carbon species concentration, however, higher plasma powers can impact the graphite quality in a negative way because of hydrogen ion etching effects. In addition, Lim's study has shown that the Ar ion density can be increased in about one order of magnitude upon increasing plasma power to 150 W.[36] Therefore, as the Raman data suggests, plasma powers below 100W are more desirable for the growth of good quality graphite. The higher defects observed in graphite films deposited at 150 W could be a result of two potential

mechanisms: (1) physical damage from energetic ions, *e.g* Ar ion bombardment;[36] (2) the etching effect caused by hydrogen ions generated by the higher plasma power. As with previous reports,[26, 39] it is believed that low plasma power is preferable in PECVD synthesis of graphite films.

4. Conclusions

In summary, we have demonstrated the synthesis of graphite films on polycrystalline Ni surfaces by IC-PECVD at low temperature ~380 °C. The graphite films grown in this work show lower Raman I_D/I_G ratio, ~0.43, compared to those reported by other groups using PECVD at higher temperatures. The Raman studies suggest that graphitic nanostructures can be synthesized on Ni after only 10 s and longer growth times lead to the formation uniform and less defective graphite films with thickness of a few nanometers. Hydrogen was found to play a key role on the quality of the graphite. In the case of hydrogen-free conditions a higher total gas pressure is needed to grow graphitic films with low I_D/I_G ratio, while lower gas pressure is preferred to deposit graphite of similar quality under hydrogen-rich conditions. The difference between the two processes is associated with the etching effect caused by excessive hydrogen ions generated by the plasma in the case of the hydrogen-rich process in comparison to the hydrogen-free process. In addition to the graphite films obtained at 380 °C, graphitic nanostructures as determined by XPS and Raman are observed at a temperature as low as 200 °C. The observation of graphitic films at such low temperature, where there is a close to zero carbon dissolubility in Ni, indicates that it is unlikely that the diffusion, segregation and precipitation growth mechanism observed at high temperature is the operating mechanism, rather the growth process proceeds by a nucleation and growth by an edge attachment process. Finally, low plasma power, about 50 W, is preferable in order to minimize the etching effect of hydrogen on the growing graphite film.

Acknowledgements

The authors would like to thank Jayhoon Chung, Cathy Vartuli and Brenda Purcell for support in TEM images. This work was financially supported by Texas Instruments and Leading Foreign Research Institute Recruitment Program (#2013K1A4A3055679) through NRF/MSIP, Korea.

REFERENCES

1. A. K. Geim and K. S. Novoselov, *Nat. Mater.*, 2007, **6**, 183.
2. H. Ago, T. Kugler, F. Cacialli, W. R. Salaneck, M. S. P. Shaffer, A. H. Windle and R. H. Friend, *J. of Phys. Chem. B*, 1999, **103**, 8116.
3. T. Gokus, R. R. Nair, A. Bonetti, M. Böhmler, A. Lombardo, K. S. Novoselov, A. K. Geim, A. C. Ferrari and A. Hartschuh, *ACS Nano*, 2009, **3**, 3963.
4. W. J. Yu, S. H. Chae, D. Perello, S. Y. Lee, G. H. Han, M. Yun and Y. H. Lee, *ACS Nano*, 2010, 4, 5480.
5. X. Wang and H. Dai, *Nat. Chem*, 2010, **2**, 661.
6. C. Chen, B. Liang, A. Ogino, X. Wang and M. Nagatsu, *J. of Phys. Chem. C*, 2009, **113**, 7659.
7. G. Zhao, D. Shao, C. Chen and X. Wang, *Appl. Phys. Lett.*, 2011, **98**, 183114.
8. F. Kreup, A. P. Graham, M. Liebau, G. S. Duesberg, R. Seidel and E. Unger, *Electron Devices Meeting, IEDM Technical Digest, IEEE International*, 2004, 683.
9. Y. Ominami, Q. Ngo, H. Yoong, A. J. Austin, A. M. Cassell, Q. Ye, J. Li, M. Meyyappan and C. Y. Yang, *Microscopy and Microanalysis*, 2005, **11**, 1964.
10. C. G. Kang, S. K. Lim, S. Lee, S. K. Lee, C. Cho, Y. G. Lee, H. J. Hwang, Y. Kim, H. J. Choi, S. H. Choe, M. H. Ham and B. H. Lee, *Nanotechnology*, 2013, **24**, 115707.
11. S. Ragan and H. Marsh, *J. Mater. Sci.*, 1983, **18**, 3161.
12. A. E. Karu and M. Beer, *J. Appl. Phys.*, 1966, **37**, 2179.
13. K. S. Kim, Y. Zhao, H. Jang, S. Y. Lee, J. M. Kim, K. S. Kim, J. H. Ahn, P. Kim, J. Y. Choi and B. H. Hong, *Nature*, 2009, **457**, 706.
14. A. Reina, X. Jia, J. Ho, D. Nezich, H. Son, V. Bulovic, M. S. Dresselhaus and J. Kong, *Nano Lett*, 2009, **9**, 30.
15. W. Liu, T. Dang, Z. Xiao, X. Li, C. Zhu and X. Wang, *Carbon*, 2011, **49**, 884.
16. S. Bhaviripudi, X. Jia, M. S. Dresselhaus and J. Kong, *Nano Lett*, 2010, **10**, 4128.
17. H. Ago, Y. Ogawa, M. Tsuji, S. Mizuno and H. Hibino, *J. Phys. Chem. Lett.*, 2012, **3**, 2228.
18. D. H. Seo, S. Kumar and K. Ostrikov, *Carbon*, 2011, **49**, 4331.
19. C. Yang, H. Bi, D. Wan, F. Huang, X. Xie and M. Jiang, *J. Mater. Chem. A*, 2013, **1**, 770.
20. G. Kalita, K. Wakita and M. Umeno, *RSC Advances*, 2012, **2**, 2815.
21. S. Wang, L. Qiao, C. Zhao, X. Zhang, J. Chen, H. Tian, W. Zheng and Z. Han, *New J. Chem.* 2013, **37**, 1616.
22. G. D. Yuan, W. J. Zhang, Y. Yang, Y. B. Tang, Y. Q. Li, J. X. Wang, X. M. Meng, Z. B. He, C. M. L. Wu, I. Bello, C. S. Lee and S. T. Lee, *Chem Phys Lett*, 2009, **467**, 361.
23. S. Z. Butler, S. M. Hollen, L. Cao, Y. Cui, J. A. Gupta, H. R. Gutie, T. F. Heinz, S. S. Hong, J. Huang, A. F. Ismach, E. Johnston-halperin, M. Kuno, V. V. Plashnitsa, R. D. Robinson, R. S. Ruoff, S. Salahuddin, J. Shan, L. Shi, O. M. G. Spencer, M. Terrones, W. Windl and J. E. Goldberger, *ACS Nano*, 2013, **7**, 2898.
24. A. Kumar, A. A. Voevodin, D. Zemlyanov, D. N. Zakharov and T. S. Fisher, *Carbon*, 2012, **50**, 1546.
25. H. K. Jeong, J. D. C. Edward, G. H. Yong and L. Choong Hun, *J. Korean Phys. Soc.*, 2011, **58**, 53.
26. L. Baraton, L. Gangloff, S. Xavier, C. S. Cojocaru, V. Huc, P. Legagneux, Y. H. Lee and D. Pribat, *Proc. of SPIE* 2009, **7399**, 73990T.
27. J. L. Qi, W. T. Zheng, X. H. Zheng, X. Wang and H. W. Tian, *Appl. Surf. Sci.*, 2011, **257**, 6531.
28. S. M. Wang, Y. H. Pei, X. Wang, H. Wang, Q. N. Meng, H. W. Tian, X. L. Zheng, W. T. Zheng and Y. C. Liu, *Journal of Physics D: Appl. Phys.*, 2010, **43**, 455402.
29. K.-J. Peng, C.-L. Wu, Y.-H. Lin, Y.-J. Liu, D.-P. Tsai, Y.-H. Pai and G.-R. Lin, *J. Mater. Chem. C*, 2013, **1**, 3862.

30 Z. Li, P. Wu, C. Wang, X. Fan, W. Zhang, X. Zhai, C. Zeng, Z. Li, J. Yang and J. Hou, *ACS Nano*, 2011, **5**, 3385.
31. R. M. Wallace, *ECS Transactions*, 2008, **16**, 255.
32. A. C. Ferrari, *Solid State Commun.*, 2007, **143**, 47.
33. M. A. Pimenta, G. Dresselhaus, M. S. Dresselhaus, L. G. Cancado, A. Jorio and R. Saito, *Phys. Chem. Chem. Phys.*, 2007, **9**, 1276.
34. S. Reich and C. Thomsen, *Phil. Trans. R. Sco. Lond. A*, 2004, **362**, 2271.
35. A. C. Ferrari, J. C. Meyer, V. Scardaci, C. Casiraghi, M. Lazzeri, F. Mauri, S. Piscanec, D. Jiang, K. S. Novoselov, S. Roth and A. K. Geim, *Phys. Rev. Lett.*, 2006, **97**, 187401.
36. Y.-D. Lim, D.-Y. Lee, T.-Z. Shen, C.-H. Ra, J.-Y. Choi and W. J. Yoo, *ACS Nano*, 2012, **6**, 4410.
37. I. Vlassiouk, M. Regmi, P. Fulvio, S. Dai, P. Datskos, G. Eres and S. Smirnov, *ACS Nano*, 2011, **5**, 6069.
38. M. Losurdo, M. M. Giangregorio, P. Capezzuto and G. Bruno, *Phys. Chem. Chem. Phys.*, 2011, **13**, 20836.
39. Y. S. Kim, J. H. Lee, Y. D. Kim, S.-K. Jerng, K. Joo, E. Kim, J. Jung, E. Yoon, Y. D. Park, S. Seo and S.-H. Chun, *Nanoscale*, 2013, **5**, 1221.
40. Y. Wang, D. C. Alsmeyer and R. L. McCreery, *Chem. Mater.*, 1990, **2**, 557.
41. T. Terasawa and K. Saiki, *Carbon*, 2012, **50**, 869.
42. Y. Kim, W. Song, S. Y. Lee, C. Jeon, W. Jung, M. Kim and C.-Y. Park, *Appl. Phys. Lett.*, 2011, **98**, 263106.
43. L. Jayeeta, S. M. Travis, J. R. Andrew, A. Lyudmyla, I. O. Ivan and B. Matthias, *New Journal of Physics*, 2011, **13**, 025001.
44. X. Li, W. Cai, L. Colombo and R. S. Ruoff, *Nano Lett.*, 2009, **9**, 4268.
45. Y. Zhang, L. Gomez, F. N. Ishikawa, A. Madaria, K. Ryu, C. Wang, A. Badmaev and C. Zhou, *J. Phys. Chem. Lett.*, 2010, 1, 3101.
46. J. J. Lander, H. E. Kern and A. L. Beach, *J. Appl. Phys.*, 1952, **23**, 1305.
47. C. Mattevi, H. Kim and M. Chhowalla, *J. Mater. Chem.*, 2011, **21**, 3324.
48. A. Malesevic, R. Vitchev, K. Schouteden, A. Volodin, L. Zhang, G. V. Tendeloo, A. Vanhulsel and C. V. Haesendonck, *Nanotechnology*, 2008, **19**, 305604.

Figure captions

Fig. 1 - Schematic diagram of the inductively coupled plasma enhanced chemical vapor deposition (IC-PECVD) system used for low temperature graphite film growth.

Fig. 2 - (a) Raman spectra of graphite films grown on polycrystalline Ni surfaces at growth temperature of 380 °C and a plasma power of 50 W using Ar:CH_4 (70:10 sccm) gas mixture as a function of time, and corresponding (b) intensity ratios of I_D/I_G and I_{2D}/I_G, and (c) FWHM of G and 2D bands.

Fig. 3 - (a) Raman mapping of the G peak intensity of graphite films after 300 s deposition time using Ar:CH_4 (70:10 sccm) gas sources at a plasma power of 50 W and growth temperature of 380 °C; (b) HR-TEM image of the graphite film after 2hrs growth time under the same deposition conditions as (a) showing thick films up to ~40 nm.

Fig. 4 - (a) Raman spectra of graphite films grown at various plasma pressures using (a) Ar:CH_4 ratio of 70:10 sccm; (c) Ar:H_2:CH_4 ratio of 30:40:10 sccm at 380 °C and a plasma power of 50W. (b) Intensity ratio of D to G bands (I_D/I_G), and (d) FWHM of G band for hydrogen-free and -rich conditions as a function of total gas pressure.

Fig. 5 - (a) Raman spectra of graphite films grown as a function of temperature on polycrystalline Ni surface under a plasma power of 50 W for 300 s and an Ar:CH_4 of 70:10 sccm; (b) corresponding Raman I_D/I_G and I_{2D}/I_G peak intensity ratios.

Fig. 6 - (a) XPS spectra of carbon 1s core level binding energy of graphite films deposited at 200, 380 and 800 °C, respectively, for 300s at a plasma power of 50 W using Ar:CH_4 (70:10) gas; and Raman spectra of graphite grown on Ni at (b) 200, 380 and 800 °C showing the higher D band intensity for the films grown at lower temperature.

Fig. 7 - (a) Raman spectra of graphite films deposited on polycrystalline Ni surface as a function of plasma power at 380 °C for 2 hrs using Ar-CH_4 gas mixture, plasma power dependent (b) intensity ratio of D to G bands and the FWHM of related G band.

Fig. S1 - Temperature dependent Raman spectra of graphite films on polycrystalline Ni surface at plasma power of 50 W for 300 s using the Ar:H_2:CH_4(40:30:10) gas mixture, (b) corresponding intensity ratios of D and 2D to G band, (c) FWHM of G band in reference to that of samples prepared using hydrogen-free (Ar:CH_4 =70:10) gas.

Fig. S2 - (a-b) SEM images of graphite films grown on polycrystalline Ni surface at 200, 380, 600 and 800 °C, respectively using Ar-CH_4 gas sources at plasma power of 50 W for 300 s.

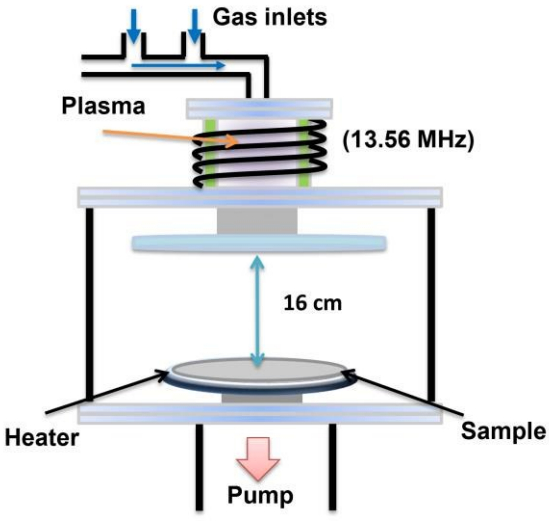

386 **Fig. 1**

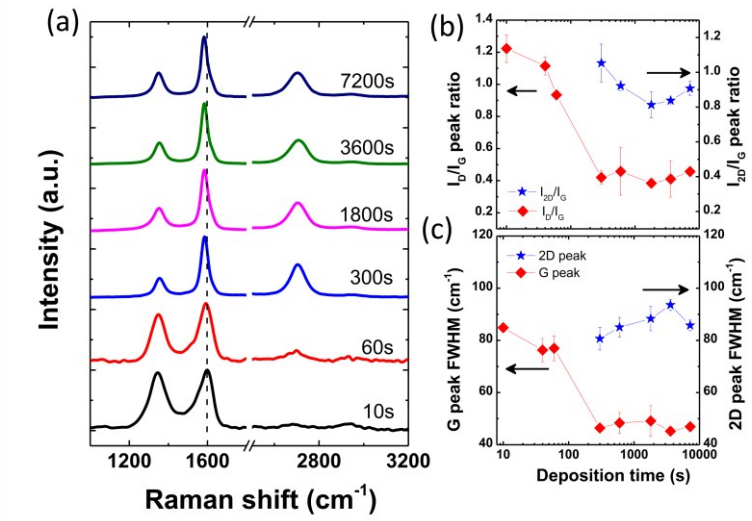

387

388 **Fig. 2**

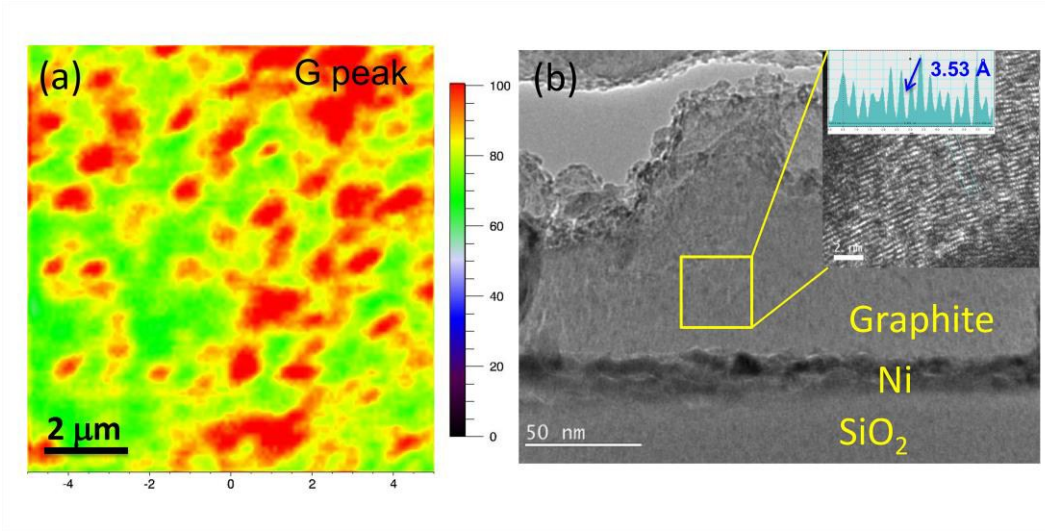

389

390 **Fig. 3**

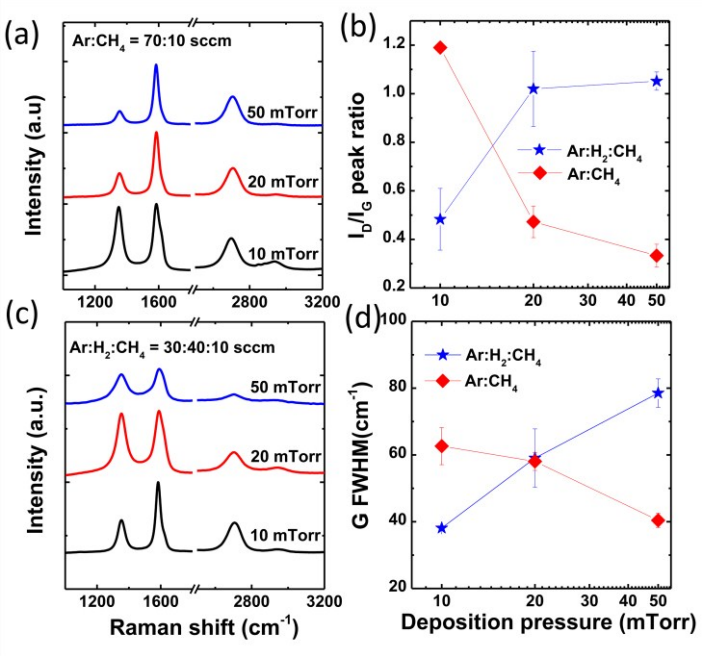

391

392 **Fig. 4**

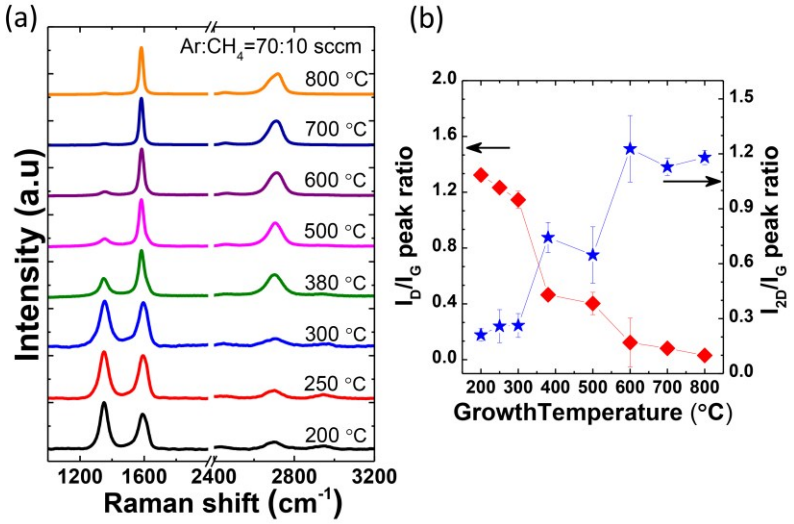

393

394 **Fig. 5**

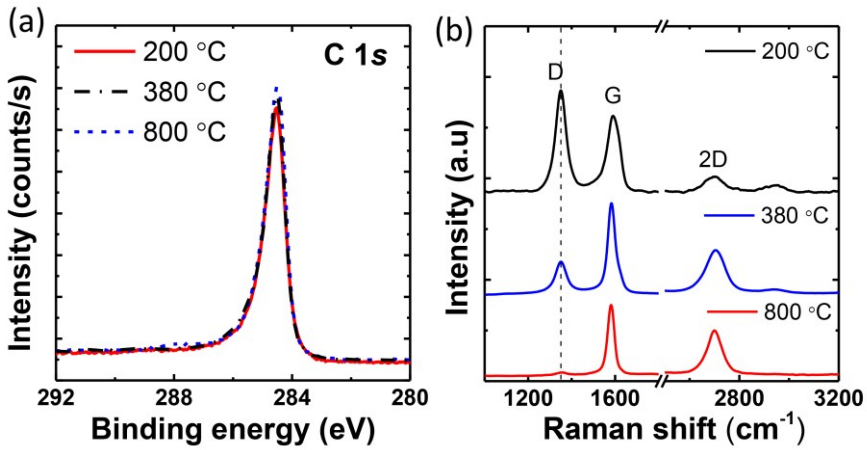

395

396 **Fig. 6**

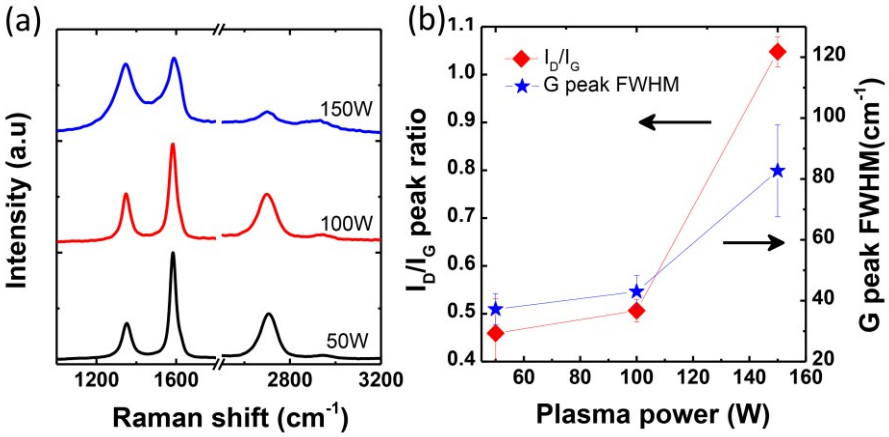

397

398 **Fig. 7**

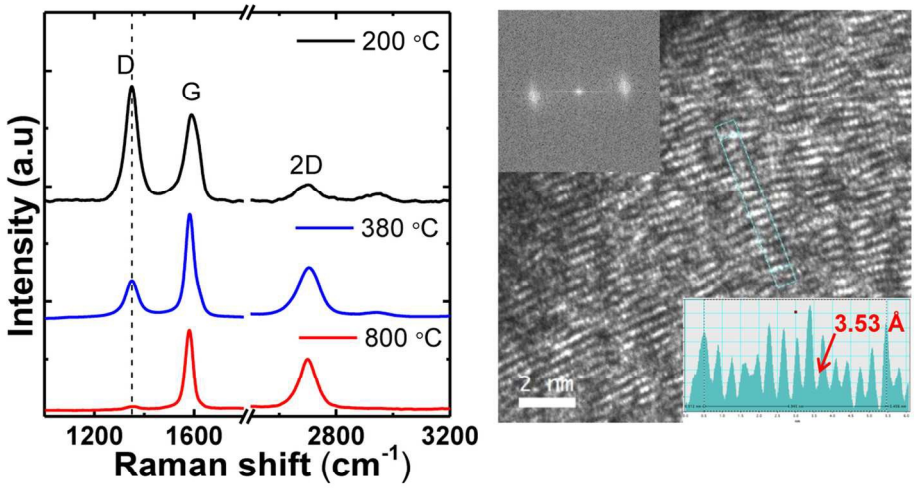

Synthesis of good quality graphite on Ni using IC-PECVD at low temperature of 380 °C in hydrogen-free environment.

114x64mm (300 x 300 DPI)